

Sea level since the Last Glacial Maximum from the Atlantic coast of Africa

Received: 28 March 2024

Accepted: 27 January 2025

Published online: 10 February 2025



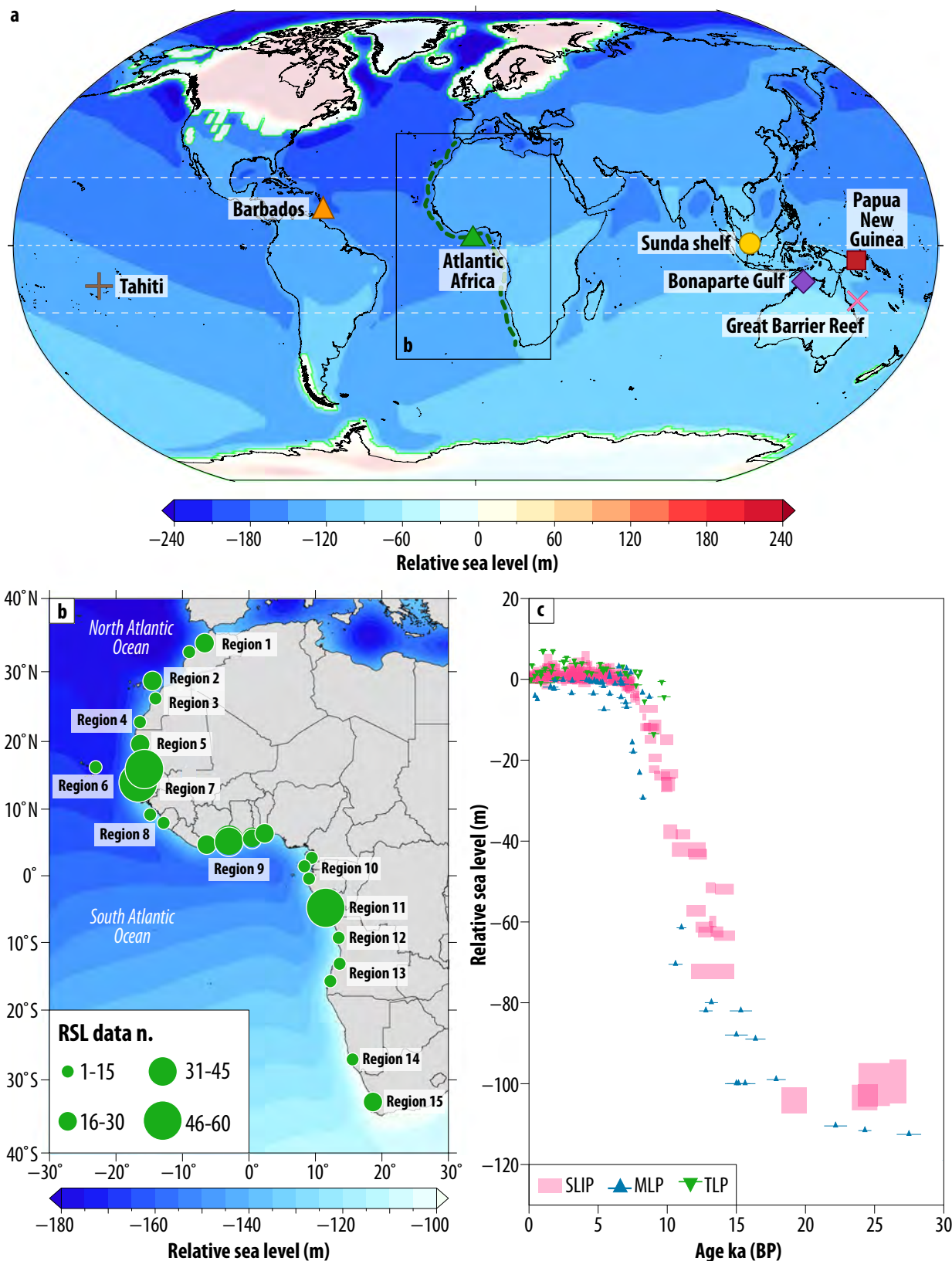
Matteo Vacchi^{1,2}✉, Timothy A. Shaw³, Edward J. Anthony⁴,
Giorgio Spada⁵, Daniele Melini⁶, Tanghua Li³, Niamh Cahill⁷ &
Benjamin P. Horton^{3,8,9}

Constraining sea level at the Last Glacial Maximum (LGM) is spatially restricted to a few locations. Here, we reconstruct relative sea-level (RSL) changes along the Atlantic coast of Africa for the last ~30 ka BP using 347 quality-controlled sea-level datapoints. Data from the continental shelves of Guinea Conakry and Cameroon indicate a progressive lowering of RSL during the LGM from -99.4 ± 5.2 m to -104.0 ± 3.2 m between ~26.7 ka and ~19.1 ka BP. From ~15 ka to ~7.5 ka BP, RSL shows phases of major accelerations up to ~ 25 mm a⁻¹ and a significant RSL deceleration by ~8 ka BP. In the mid to late Holocene, data indicate the emergence of a sea-level highstand, which varied in magnitude (0.8 ± 0.8 m to 4.0 ± 2.4 m above present mean sea level) and timing (5.0 ± 1.0 to 1.7 ± 1.0 ka BP). We further identified misfits between glacial isostatic adjustment models and the highstand, suggesting the interplay of different ice-sheet meltwater contributions and hydro-isostatic processes along the wide region of Atlantic Africa are not fully resolved.

Projections of future sea levels rely on the understanding the relationship between sea levels with past climate and global ice volumes¹. In particular, reconstructions of relative sea-level (RSL) change from far-field regions (i.e., located far from extinct ice sheets) since the Last Glacial Maximum (LGM) provide fundamental constraints to global ice volumes^{1,2} and isostatic response of the solid Earth to the large ice-ocean mass redistribution^{3,4}. Most published sea-level records are temporally restricted to the Holocene⁵ (last ~11.7 ka BP) with very few extending to the LGM^{2,6,7} (e.g., last ~30 ka BP). Indeed, there is an absence of quality-controlled LGM data from the Atlantic Ocean except for the Barbados record (Fig. 1a), which has been central to constraining the timing and magnitude of the LGM lowstand^{2,8,9} and the existence of Meltwater Pulse events including 1b (MWP1b)^{10,11}. Data on the spatial and temporal variability of the mid-Holocene sea-level highstand are also only presently available for the South American and Caribbean coasts of the western Atlantic Ocean^{12–14}.

Here, we compiled a quality-controlled RSL database since the LGM from the Atlantic coast of Africa (Fig. 1a), a passive margin mostly characterized by minor late Quaternary tectonic activity^{15–17}. We produced 234 Sea Level Index Points (SLIPs that constrain RSL in time and space with quantifiable uncertainty¹⁸) and 113 terrestrial and marine limiting points (points that constrain the upper and lower boundary of RSL, respectively¹⁸). We clustered the database into 15 regions (Fig. 1b) based on their geographic location^{19–21} (see Methods). We quantified RSL changes using an Error-In-Variables Integrated Gaussian Process (EIV-IGP) model²² and compared the reconstructed RSL histories with GIA predictions from the ICE-6G (VM5a)²³ and ANU^{24,25} models to: (1) constrain the timing and magnitude of RSL changes during the LGM (~29.5 ka to ~19.0 ka BP); (2) quantify magnitudes and rates of postglacial RSL change; and (3) probabilistically define the timing and magnitude of the Holocene sea-level highstand in the last 8.0 ka BP.

¹Dipartimento di Scienze Della Terra, Università di Pisa, Via S. Maria, 53, Pisa, Italy. ²Istituto di Geoscienze e Georisorse, National Research Council, Via G. Moruzzi 1, Pisa, Italy. ³Earth Observatory of Singapore, Nanyang Technological University, Singapore, Singapore. ⁴Aix Marseille Université, CNRS, IRD, INRAE, Coll France, CEREGE, Aix-en-Provence, France. ⁵Dipartimento di Fisica e Astronomia “Augusto Righi” (DIFA), Alma Mater Studiorum - Università di Bologna, Bologna, Italy. ⁶Istituto Nazionale di Geofisica e Vulcanologia, Via di Vigna Murata 605, Roma, Italy. ⁷Department of Mathematics and Statistics, Maynooth University, Maynooth, Kildare, Ireland. ⁸Asian School of the Environment, Nanyang Technological University, Singapore, Singapore. ⁹School of Energy and the Environment, City University of Hong Kong, Kowloon, Hong Kong. ✉e-mail: matteo.vacchi@unipi.it



Results and discussions

Sea-level evolution during the Last Glacial Maximum and the Late-glacial period

The timing, magnitude and rate of RSL changes during the LGM and late-glacial period (i.e., from the onset of the LGM at -29.5 ka BP to the beginning of the main phase of deglaciation at -16.5 ka BP^{24,26,27})

represents a key time period to constrain the progressive melting of polar ice-sheets²⁷.

The production of a suite of SLIPs ($n=4$) and marine limiting points ($n=5$) collected from the continental shelf of Guinea Conakry (region 8), Ivory Coast (region 9) and Cameroon (region 10) constrain RSL change in the Atlantic Ocean between -29.5 ka and -16.5 ka BP

Fig. 1 | Geographical and chronological extent of the Relative Sea Level (RSL) dataset used for our analysis. a Spatial distribution of the Last Glacial Maximum (LGM) and Late-Glacial sea-level records from far-field regions presently available in the literature (Barbados², Bonaparte Gulf⁶, Great Barrier Reef⁷, Sunda Shelf²⁸, Tahiti²⁹). The dotted green line indicates the extension of the coastline investigated in this study. Bright green outline with white shading represents the extent of ice coverage at the LGM in ICE-6G, **b** Geographical distribution of the sea-level

datapoints for Atlantic Africa. Numbers indicate the location of the 15 regions. **c** Total plot of the RSL datapoints along the Atlantic margin of Africa. RSL source data are provided as a Source Data file. SLIP is the Sea-level Index point, TLP is the Terrestrial Limiting Point, and MLP is the Marine Limiting Point. Dimensions of boxes and lines for each point based on 2σ elevation and age uncertainties. The scale bar in panels **a** and **b** is the RSL predictions at the LGM (i.e., 26 ka BP) from the glacial isostatic adjustment model ICE-6G. Source data are provided as a Source Data file.

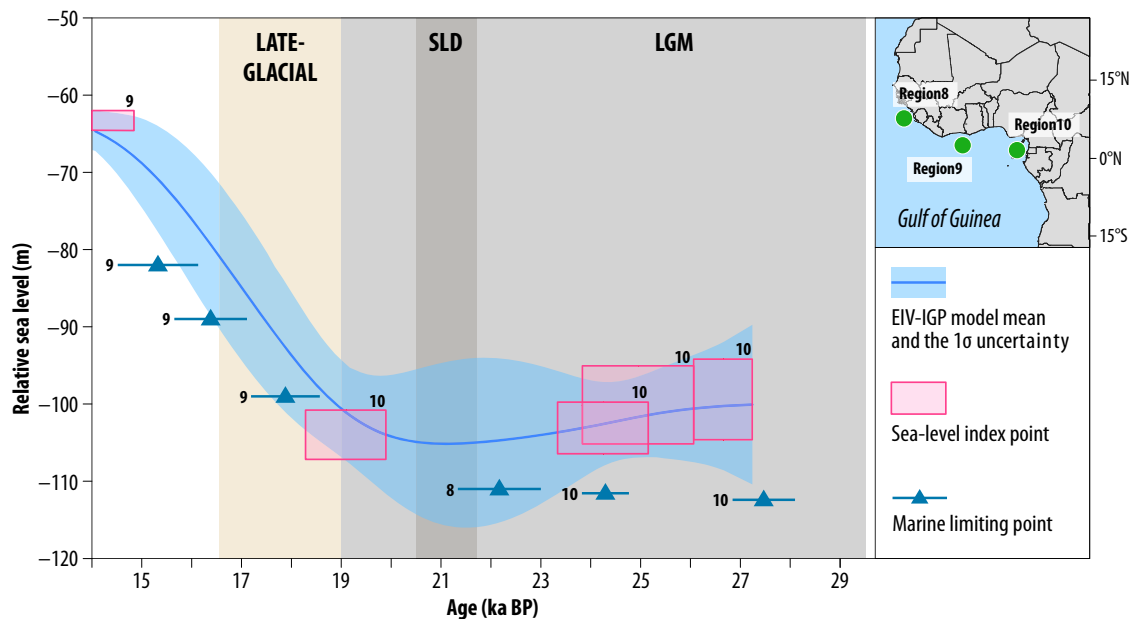


Fig. 2 | Relative Sea Level (RSL) datapoints and EIV-IGP model prediction between 28 ka and 14 ka BP. Datapoints are from the continental shelf of Guinea Conakry (region 8), the northern Gulf of Guinea (region 9), and Cameroon (region 10). The shaded grey and shaded brown areas indicate the extent of the Last Glacial Maximum and Late-Glacial periods^{26,27}. The dark grey area indicates the timing of

the sea-level drop recorded in the Great Barrier Reef⁷. The blue solid line and shaded envelope denote the EIV-IGP model mean and the $\pm 1\sigma$ uncertainty. SLD indicates the timing of the Sea Level Drop recorded in the Great Barrier Reef⁷. Source data are provided as a Source Data file.

(Fig. 2). During the LGM period (~ 29.5 ka to ~ 19.0 ka BP), RSL fell from -99.4 ± 5.2 m at 26.7 ± 0.6 ka BP to -103.1 ± 3.2 m at 24.2 ± 0.9 ka BP (Fig. 2). Between ~ 24 ka and ~ 20 ka BP, RSL is constrained by a single marine limiting point above -111 ± 2.4 m at 22.1 ± 0.8 ka BP while a SLIP shows RSL was at -104 ± 3.2 m at 19.1 ± 0.8 ka BP. The EIV-IGP model indicates rates of RSL fall of 1.0 ± 4.3 mm a^{-1} between ~ 27 ka and ~ 24 ka BP, and 0.8 ± 4.4 mm a^{-1} between ~ 24 ka and ~ 19 ka BP. In the Late-glacial period (19 ka to 16.5 ka BP), SLIPs and marine limiting data indicate RSL rose from above -99 ± 1.2 m at 17.8 ± 0.7 ka BP to above -89 ± 1.2 m at 16.3 ± 0.7 ka BP at a maximum rate of 9.0 ± 4.7 mm a^{-1} .

The lowering of RSL from ~ 26.6 ka to ~ 19.8 ka BP indicated by Atlantic coast of Africa data suggests a sea-level minimum at the end of the LGM (~ 21 ka to ~ 20 ka BP), which has also been inferred from the records collected in the Indo-Pacific regions^{6,7,28}. This lowering supports an increasing ice volume driven by the eastward and southward expansion of the Scandinavian ice sheet as well as the southward advance of the Laurentide ice sheet^{24,25}. The lack of data between 22 ka and 20 ka BP did not allow the identification of an abrupt ~ 40 m drop in RSL at ~ 21 ka BP that was recorded in the Great Barrier Reef⁷.

These data represent the first Atlantic Ocean evidence of the sea-level lowering trend during the LGM. Previously, the Barbados record, was the single LGM dataset available for the Atlantic Ocean^{2,8,10} but its accuracy in defining the timing and magnitude of the LGM was debated for possible tectonic influence⁸ as well as for the potential presence of allochthonous dated material from downslope transportation of the coral sea-level indicators²⁹.

Rates of sea-level rise during the main phase of deglaciation

A major phase of deglaciation and consequent increase in global mean sea level occurred between ~ 16.5 ka and ~ 7.0 ka BP²⁴ from a reduction of land-based ice volume of $\sim 45 \times 10^6$ km³.

The presence of numerous SLIPs ($n = 42$) from Senegal (region 7), northern Gulf of Guinea (region 9) and Congo (region 11) enabled the quantitative assessment of magnitudes and rates of RSL change along a large portion of the Atlantic coast of Africa. In Senegal, RSL rose from -53.6 ± 3.5 m at 14.8 ± 0.2 ka BP to -39.2 ± 4.0 m at 11.5 ± 0.2 ka BP and to -1.24 ± 0.7 m at 7.0 ± 0.2 ka BP (Fig. 3a). The 24 SLIPs record a progressive increase in sea-level rate rising at 9 to 11 mm a^{-1} between 11.5 ka and 8.5 ka BP and decreasing to $<7.0 \pm 1.0$ mm a^{-1} after 8.0 ka BP (Fig. 3b).

In the northern Gulf of Guinea, RSL was stable at -61.6 ± 3.0 m between 14.0 ka and 13.0 ka BP (Fig. 3c). RSL rose to -44.9 ± 4.0 m at 12.0 ± 0.2 ka BP and to -37.2 ± 3.0 m at 11 ± 0.2 ka BP. Younger SLIPs indicate RSL rose to -6.1 ± 0.2 m at 8.0 ± 0.2 ka BP and finally to -1.6 ± 0.7 m at 7.0 ± 0.2 ka BP. The 9 SLIPs indicate two phases of major acceleration with rates of rise up to 25.2 ± 11 mm a^{-1} between 12.6 ka and 12.1 ka BP and up to 11.6 ± 11 mm a^{-1} between 10.0 ka and 8.0 ka BP (Fig. 3d). After 8.0 ka BP, RSL rates were $<7.0 \pm 2$ mm a^{-1} at 7.5 ka BP.

In Congo, RSL rose from -70.7 ± 3.9 m to -24.7 ± 1.7 m between 13.3 ± 0.2 ka and 10.0 ± 0.2 ka BP (Fig. 3e). Younger SLIPs indicate RSL rose to -4.3 ± 2.0 m at 8.0 ± 0.2 ka BP and reached present sea-level at 7.0 ka BP. The 9 SLIPs show sea-level rise at rates from 13.4 ± 3.4 mm a^{-1} at 13.0 ka BP to 14.8 ± 1.8 mm a^{-1} at 11.4 ± 0.2 ka BP (Fig. 3). This was followed by progressive decrease in rising rates from 10.3 ± 1.4 mm a^{-1} after 9.0 ka BP to 6.0 ± 1.0 mm a^{-1} after 8.0 ka BP, respectively (Fig. 3f).

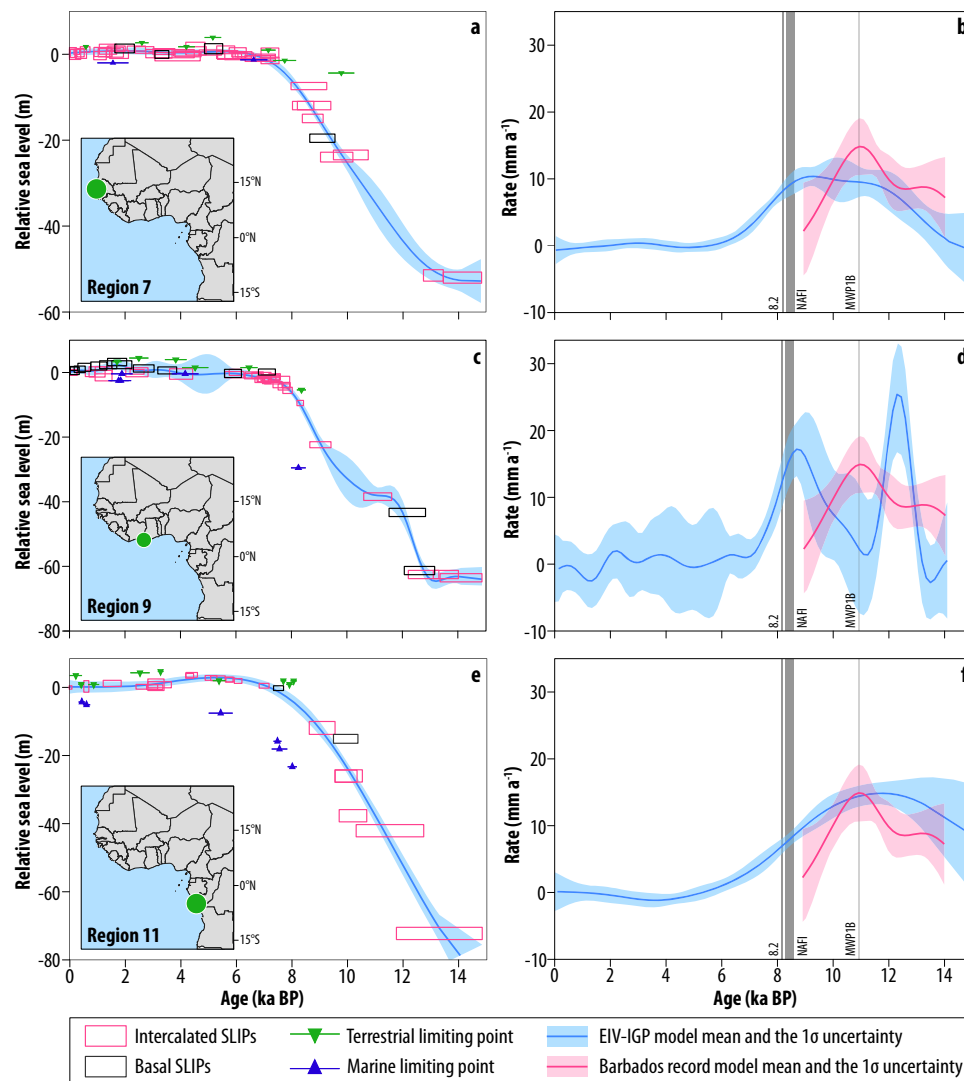


Fig. 3 | Quantitative reconstruction of Relative Sea Level (RSL) position and rates of RSL changes during the main phase of deglaciation. a, c, e RSL data and EIV-IGP model predictions in Senegal (region 7), northern Gulf of Guinea (region 9) and Congo (region 11). Green dots indicate region locations. Black boxes are basal sea-level index points (SLIPs). Pink boxes are intercalated SLIPs. Limiting points are plotted as green (terrestrial) or blue (marine) triangles with horizontal lines. Dimensions of boxes and lines for each point based on 2σ elevation and age uncertainties. The blue solid line and shaded envelope denote the EIV-IGP model

mean and the $\pm 1\sigma$ uncertainty. **b, d, f** Statistical reconstruction of the rates of RSL change for Senegal (region 7), northern Gulf of Guinea (region 9) and Congo (region 11). The pink solid line and shaded envelope denote the Barbados record EIV-IGP model mean and the $\pm 1\sigma$ uncertainty. MWPIb is the Meltwater Pulse 1b. The grey bands indicate the temporal extent of the North Atlantic Freshwater input (NAFI) and of the 8.2 ka cooling event^{27,32}. Source data are provided as a Source Data file.

The postglacial records from Senegal, the northern Gulf of Guinea, and Congo offer the opportunity to investigate the evidence for MWP events including MWPIb, the existence of which has been debated^{10,11,29}. MWPIb is a rapid acceleration of sea-level identified in the Barbados record between 11.5 ka and 11.0 ka BP^{10,29}. Evidence for this major acceleration, however, is not recorded in Senegal (Fig. 3b) or Congo (Fig. 3f). An acceleration is recorded in the northern Gulf of Guinea (Fig. 3d), but its timing (12.6 ka to 12.1 ka BP) is ~1.0 ka older than the reported occurrence of MWPIb derived from the Barbados record¹⁰. This reconstruction, however, is based on a limited number of SLIPs ($n = 6$) between ~15 ka and ~10 ka BP, some with large temporal (i.e., ± 0.6 ka) and vertical (i.e., ± 1.7 m) uncertainties. Our interpretation of rapid increases in sea level during this period are, therefore, restrained until further evidence is found.

In Senegal and in the northern Gulf of Guinea we observe peak rates of sea-level rise preceding the 8.2 ka cooling event triggered by North Atlantic Freshwater Input following the collapse of North

American proglacial Lake Agassiz/Ojibway and of the Hudson Bay Ice Saddle^{30–32}. The low temporal resolution of our sea-level data, however, does not allow for a clear identification of the rapid sea-level acceleration precluding the 8.2 ka event as identified in the Netherlands^{33,34}, Scotland^{32,35}, Chesapeake Bay³⁶, and the Mississippi delta³⁷.

Indeed, the quantitative reconstructions from Senegal and northern Gulf of Guinea clearly identify a major deceleration of rising rates after ~8.0 ka (Fig. 3b,d), whose timing is consistent with the global decrease in rates between 8.2 ka and 6.7 ka BP consequent to the final phase of North American deglaciation²⁴.

Timing and magnitude of the sea-level highstand

In far-field regions, the coupled activity of ocean syphoning (i.e., the migration of water from far-field regions into areas vacated by fore-bulge collapse and subsidence at the periphery of deglaciation centres to maintain dynamic equilibrium^{31,2}) and continental levering (i.e., vertical land motion of continental margins due to the increasing

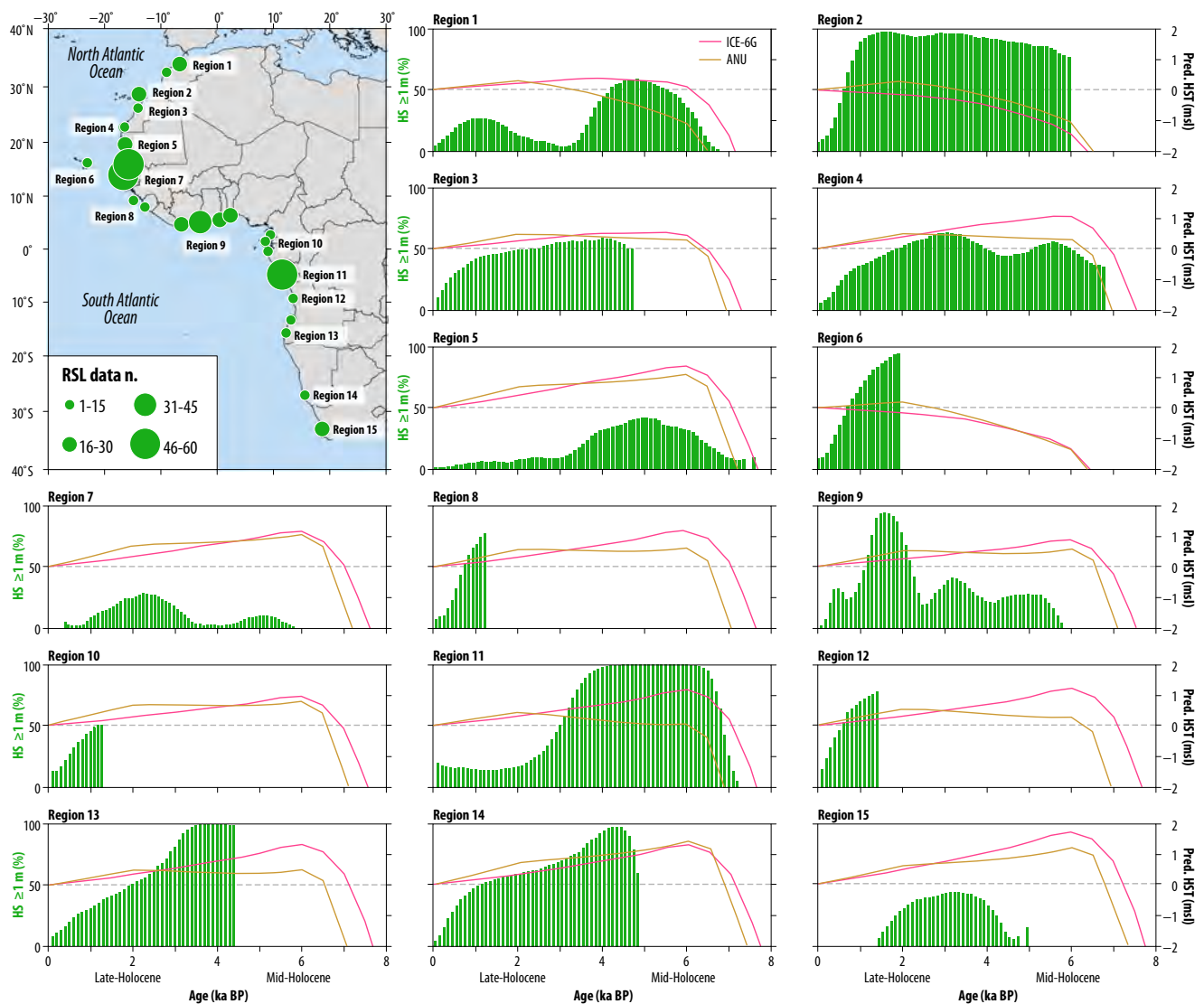


Fig. 4 | Probability of a Holocene sea-level highstand (HS) ≥ 1 m along the Atlantic coast of Africa. Data are plotted against the ICE-6G (pink line) and ANU (yellow line) RSL predictions in the 15 regions of Atlantic Africa. Source data are provided as a Source Data file.

ocean loading caused by rising sea levels, which induces subsidence of offshore regions and an uplift of onshore regions^{3,12}) result in the emergence of a sea-level highstand. Understanding variability in the timing and magnitude of highstand formation is fundamental to constrain Earth and ice model parameters in GIA modelling^{3,38}.

The dense concentration of SLIPs ($n = 203$, Fig. 1b) in all 15 regions of the Atlantic coast of Africa during the mid- to late-Holocene enables a quantitative assessment of magnitudes and rates of RSL change as well as comparisons with predictions from the ICE-6G and ANU models (Fig. 4 and Supplementary 1).

In Mauritania and Senegal (regions 5 and 7), the probability of a highstand ≥ 1 m is $\leq 50\%$ while along most of northernmost sector of Atlantic coast of Africa (regions 1 to 4), the Sierra Leone and northern Gulf of Guinea (regions 8 and 9) and the southernmost sector (regions 11, 13 and 14) the probability of a highstand ≥ 1 m is $\geq 50\%$ (Fig. 4). Both GIA models predict the formation of a highstand above present level in most of the Atlantic coast of Africa (see Supplementary Figs. 2, S2_1 and S2_2). However, both the timing and magnitude of the highstand show differences between the ICE-6G and ANU predictions. ICE-6G predicts a single maximal highstand followed by a continuous drop in RSL for the remaining part of the Holocene. The maximal highstand is generally predicted at ~ 6.0 ka BP and its magnitude is ≥ 1 m in most of

the regions with the exception of the northernmost portion of Atlantic coast of Africa (northern Morocco, region 1 and northern Atlantic Sahara, region 3) where the highstand is predicted above present level but ≤ 1 m and in the offshore archipelagos of the Canary Islands and Cabo Verde (regions 2 and 6) where no highstand is predicted. ANU predictions, however, show a more variable pattern of RSL change. At latitudes higher than $\sim 25^\circ\text{N}$ (e.g., region 1 and 3) and in the offshore archipelago of the Canary Islands and Cabo Verde (regions 2 and 6), the maximal highstand is predicted at ~ 2.0 ka BP and always < 1 m above present level. The remaining regions are generally characterized by a highstand at ~ 6.0 ka BP, which is followed by minor fluctuations in RSL until a second highstand which formed at ~ 2.0 ka BP. The elevation of the highstand at ~ 6.0 ka BP is ≥ 1 m above present level only in Mauritania, Senegal, southern Namibia and South Africa (regions 5, 6, 14 and 15). The highstand at ~ 2.0 ka BP is always ≤ 1 m and its maximal elevations (0.5 to 0.7 m above the present datum) are predicted in the coastal sector between Senegal and Cameroon (regions 7, 8, 9, 10).

Our RSL reconstructions indicate the establishment of mid-Holocene highstands ≥ 1 m in the northernmost sector of Atlantic coast of Africa at latitudes between 35°N and 26°N (Fig. 4). Both ICE-6G and ANU model predictions show misfits in both the timing and the magnitude of this highstand formation (Fig. 4). This misfit may be due

to the neglect of 3D (i.e., lateral heterogeneous) Earth structure, which is important for continental-scale studies of GIA^{39,40}. Notably, the potential lateral viscosity variations inferred from shear velocity anomalies in seismic tomography model across the Atlantic coast of Africa are significant⁴¹. Alternatively, it might be an underestimation of the ice-equivalent sea level contribution from North America which is not compensated by an Antarctic contribution in both of the GIA models (Supplementary Figs. 2, S2.1 and S2.2). This underestimation of the ice-equivalent sea level contribution would result in the formation of a mid-Holocene highstand in the northernmost sector of Atlantic coast of Africa whose chronology is comparable with the highstand observed at lower latitudes (-8° to -5° N; Guyana and Suriname) and South America¹³.

Between -15° N and -0° (Regions 6 to 10, Fig. 4 and Supplementary Figs. 1, S1.2) data indicate RSL reached its maximal elevation above the present sea-level in the late Holocene (-2.0 to -1.7 ka BP). The emergence of this highstand is not predicted by ICE-6G while ANU model predicts a late Holocene highstand in all these regions but at elevations always ≤ 1 m (Fig. 4). However, the probabilistic analysis (Fig. 4) suggests this highstand exceeded 1 m in Cabo Verde Islands (Region 6, highstand ≥ 1 m = 92%), Sierra Leone (Region 8, highstand ≥ 1 m = 77%) and Gulf of Guinea (region 9 = highstand ≥ 1 m = 91%). With the sole exception of the volcanic archipelago of Cabo Verde, the current elevation of this highstand is difficult to explain solely through post-depositional vertical ground movements, given the low Quaternary tectonic activity observed along the Atlantic coast of Africa^{15,16,42}.

The emergence of this highstand is most likely driven by hydro-isostatic processes (including ocean syphoning and continental levering), whose timing and magnitude is mainly controlled by the deglaciation history and Earth (i.e., viscosity) structure³⁸. For example, the meltwater input from Antarctic ice sheet diminished over the last -7.5 ka, although the exact timing and relative contributions are not fully resolved^{23,43,44}. The timing of the Antarctic ice-sheet melting represents a major difference between the models employed in our analysis. In ICE-6G, the Antarctic contribution to meltwater input is minimal in the late Holocene while for ANU the contribution lasted until -2.0 ka BP (Supplementary 2, Figure S2.3). The isostatic response of the far-field regions of Atlantic coast of Africa supports that ice volumes were still changing in some regions of Antarctica in the late-Holocene^{44–46}. In particular, the Antarctic Thermal Optimum^{47,48} stimulated melt of the western Antarctic ice sheet until to 2.0 ka BP²⁴, although increased ice accumulation rates in the interior of western Antarctica from warmer temperatures and higher precipitation had implied an ice mass expansion⁴⁹. Our data imply that the dynamic contributions from Antarctica may be missing (for ICE-6G) or underestimated (for ANU models) from the ice histories used in global GIA models in the mid to late Holocene^{50,51}.

Methods

Compilation of a deglacial sea-level database for the Atlantic coast of Africa

The Atlantic Africa database of SLIPs and marine and terrestrial limiting points was assembled following protocols described by the International Geoscience Programme (IGCP) projects⁵², and INQUA project HOLSEA^{5,53}. A SLIP estimates the unique position of RSL in space and time with corresponding vertical and temporal uncertainties^{18,21}. Where a suite of SLIPs exists for a locality or region, they indicate changes in RSL through time and allow the magnitude and rate of RSL change to be estimated¹⁹. Limiting points provide an upper (terrestrial or upper limiting data points) or lower (marine or lower limiting data points) bound on the past position of RSL at a given point in space and time⁵².

The sea-level datapoints were extracted from a wide range of published studies carried out along the Atlantic Africa coasts since the 1960s^{54–77}. A wide range of sea-level indicators characterize the Atlantic

coast of Africa (Supplementary Tables 3, S3.2). These can be subdivided in: i) low-energy sea-level indicators derived from cores or exposures found in coastal marshes, *sebkhas* and lagoons^{54–57,77}; ii) low-energy sea-level indicators derived from off-shore coring performed along the continental shelf^{58–60}; iii) high-energy sea-level indicators derived from beachrocks or loose beach deposits including beach ridges^{61–64,77} and iv) sea-level indicators derived from fossil bioconstructions^{65,66}. The indicative meaning of SLIPs (i.e., the quantitative relationship between the dated facies and the contemporary tidal frame^{52,53}) were estimated using published data relating the modern elevational distribution of faunal assemblages^{54,67,68} and/or based on the sediment bedding architecture (for beachrocks and loose beach deposits). Detailed descriptions of the indicative meaning of the different sea-level indicators are provided in Supplementary Tables 3, S3.2. Marine limiting points were mainly from samples found in infralittoral (subtidal) sedimentary facies^{59,69,70} while terrestrial limiting points were from samples found in facies dominated by freshwater plant macrofossils as well as dune and fluvial facies^{66,71,72}. Samples provided by archaeological middens from prehistoric coastal settlements^{73,74} were transformed into terrestrial limiting points with the exception of a suite of data from the Banc d'Arguin (Mauritania) which have a quantitative relationship with the former tidal frame and were transformed in SLIPs⁷⁵. Data from Namibia and South Africa were extracted from the recent database produced using the Holsea guidelines⁷⁶.

We subdivided the SLIPs derived from cores into basal and intercalated categories to assess the influence of sediment compaction⁷⁸. Basal samples are those recovered from within the sedimentary unit that overlies the incompressible substrate and are less prone to sediment compaction. SLIPs derived from beach deposits, beachrocks and vermetid reefs are classified as basal because they are compaction-free⁷⁸. Where stratigraphic information was unavailable for a SLIP, we conservatively interpreted it as intercalated.

We calibrated the age of all samples in the Atlantic Africa database using CALIB 8.2 with a 2σ range and employed the IntCal20⁷⁹, SHCal20⁸⁰ and Marine20⁸¹ calibration curves for terrestrial samples and marine samples, respectively. Where available, information on the necessary reservoir correction was taken from the Marine Reservoir Database⁸¹. All SLIPs are presented as calibrated years before present (BP), where the reference epoch is 1950 AD. A concern with old radiocarbon ages is the correction for isotopic fractionation⁸². This became a standard procedure in most laboratories by the late 1970s, but some laboratories have only applied this correction since the mid-1980s¹⁸. In the database, a significant number of samples were analysed before 1990 and, therefore, we followed the procedure of the HolSEA protocol⁵ to correct for isotopic fractionation. We finally discarded 87 SLIPs and limiting points because of the following reasons: (i) difficulties in definition of the indicative meaning, (ii) difficulties in defining the elevation of the sample, (iii) major compaction of intercalated samples, (iv) anomalous RSL when compared to coeval data from the same region.

The Atlantic Africa has a N-S orientation except for the northern side of the Gulf of Guinea (e.g., from Ivory Coast to the Niger delta), which runs W-E. We clustered the RSL data into 15 regions based and on their distance from the palaeo-ice sheets^{19–21}. A detailed description of the tectonic, geographic, and climatic setting of these regions is provided in Supplementary 3.

Statistical modelling and GIA predictions

In each of the 15 regions, the quantitative reconstruction of RSL evolution was performed by applying the EIV-IGP model²². The EIV (errors-in-variables)⁸³ accounts for error due to radiocarbon age uncertainties, and the IGP (integrated Gaussian process) is useful for modelling non-linear trends in data. The EIV-IGP model evaluates RSL and its rate of change over time by assuming a prior Gaussian process specified by a

mean function and a covariance function that smooths the RSL reconstructions. The model is flexible, capable of accommodating missing data, and enables probabilistic inferences about RSL change over time²². We modelled RSL changes every 150 years and the final accuracy of our reconstruction is dependent on the number of SLIPs in a given timespan and their vertical and horizontal uncertainty.

To better examine the spatial and temporal variability of the sea-level highstand, we used the EIV-IGP model to analyze the probability of RSL being ≥ 1 m which is the average elevation predicted by the suite of GIA models along the Atlantic coast of Africa (see supplementary 2).

The GIA predictions were obtained by solving the gravitationally and topographically self-consistent Sea-Level Equation (SLE)⁸⁴. The SLE, which describes the spatiotemporal variations of sea-level associated with the melting of late Pleistocene ice sheets, has been solved numerically using the SELEN4 open-source code^{85,86}. SELEN4 assumes a laterally homogeneous, spherical, incompressible, and self-gravitating Earth characterized by a Maxwell rheology. It includes the effects of rotational feedback on sea level⁸⁷ and accounts for horizontal migration of shorelines⁸⁸. We have implemented in SELEN4 realizations of three different GIA models: *i*) the ICE-6G²³ spatio-temporal evolution of ice sheets, coupled with a five-layer approximation of the VM5 viscosity profile⁸⁸, in which the thickness of the elastic lithosphere has been kept constant to 90 km, the upper mantle and transition zone viscosities have been set to 5×10^{20} Pa-s, while the lower mantle has been approximated with two homogeneous layers of viscosities 1.5×10^{21} Pa-s and 3.2×10^{21} Pa-s⁸⁹; *ii*) two versions of the ANU global GIA model, corresponding to the “high-viscosity” and “low-viscosity” solutions obtained by Kurt Lambeck and collaborators²⁴, in which the thickness of the elastic lithosphere and upper mantle viscosities have been set to 60 km and 1.5×10^{20} Pa-s, respectively, while for the lower mantle we considered both the low-viscosity (2.0×10^{21} Pa-s, ANUlv) and the high-viscosity (7.0×10^{22} Pa-s, ANUlv) values. In all the figures of the manuscript, we only show the ANUlv predictions which showed a better agreement with the suites of sea-level data. For all the considered GIA models, the present-day topography has been prescribed according to the bedrock version of the ETOPO1 global topographic model⁹⁰, integrated with the Bedmap2 relief⁹¹ in the Antarctica region (i.e., below 60°S latitude). The numerical solutions of the SLE have been obtained on a global geodesic grid with spatial resolution of ~40 km and include harmonic terms up to harmonic degree $L_{MAX} = 512$, corresponding, by Jeans rule, to the minimum wavelength of ~80 km over the Earth’s surface.

Data availability

The RSL database generated in this study and the outputs of the quantitative reconstruction of RSL evolution are provided in the Source Data file. The database of Atlantic Africa sea-levels is also available at https://github.com/matteovacchi/Sea_levels_Atlantic_Africa. The output of the GIA models are available by request. The present-day topography used for GIA models is available at www.ncei.noaa.gov and www.bas.ac.uk/project/bedmap-2/. Source data are provided with this paper.

References

- Bassett, S. E., Milne, G. A., Mitrovica, J. X. & Clark, P. U. Ice sheet and solid earth influences on far-field sea-level histories. *Science* **309**, 925–928 (2005).
- Peltier, W. R. & Fairbanks, R. G. Global glacial ice volume and Last Glacial Maximum duration from an extended Barbados sea level record. *Quat. Sc. Rev.* **25**, 3322–3337 (2006).
- Mitrovica, J. X. & Milne, G. A. 2002. On the origin of late Holocene sea-level highstands within equatorial ocean basins. *Quat. Sc. Rev.* **21**, 2179–2190 (2002).
- Milne, G. A., Gehrels, W. R., Hughes, C. W. & Tamisiea, M. E. Identifying the causes of sea-level change. *Nat. Geosci.* **2**, 471–478 (2009).
- Khan, N. S. et al. Inception of a global atlas of sea levels since the Last Glacial Maximum. *Quat. Sci. Rev.* **220**, 359–371 (2019).
- Ishiwa, T. et al. Reappraisal of sea-level lowstand during the Last Glacial Maximum observed in the Bonaparte Gulf sediments, northwestern Australia. *Quat. Int.* **397**, 373–379 (2016).
- Yokoyama, Y. et al. Rapid glaciation and a two-step sea level plunge into the Last Glacial Maximum. *Nature* **559**, 603–607 (2018).
- Austermann, J., Mitrovica, J. X., Latychev, K. & Milne, G. A. Barbados-based estimate of ice volume at Last Glacial Maximum affected by subducted plate. *Nat. Geosci.* **6**, 553–557 (2013).
- Nakada, M., Okuno, J. I. & Yokoyama, Y. Total meltwater volume since the Last Glacial Maximum and viscosity structure of Earth’s mantle inferred from relative sea level changes at Barbados and Bonaparte Gulf and GIA-induced \dot{J} 2. *Geophys. J. Int.* **204**, 1237–1253 (2016).
- Abdul, N. A., Mortlock, R. A., Wright, J. D. & Fairbanks, R. G. Younger Dryas sea level and meltwater pulse 1B recorded in Barbados reef crest coral *Acropora palmata*. *Paleoceanography* **31**, 330–344 (2016).
- Bard, E., Hamelin, B., Deschamps, P. & Camoin, G. Comment on “Younger Dryas sea level and meltwater pulse 1B recorded in Barbados reefal crest coral *Acropora palmata*” by NA Abdul et al. *Paleoceanography* **31**, 1603–1608 (2016).
- Milne, G. A., Long, A. J. & Bassett, S. E. Modelling Holocene relative sea-level observations from the Caribbean and South America. *Quat. Sci. Rev.* **24**, 1183–1202 (2005).
- Khan, N. S. et al. Drivers of Holocene sea-level change in the Caribbean. *Quat. Sci. Rev.* **155**, 13–36 (2017).
- Paniagua-Aroyave, J. F., Spada, G., Melini, D., & Duque-Trujillo, J. F. Holocene relative sea-level changes along the Caribbean and Pacific coasts of northwestern South America. *Quat. Res.* **119**, 28–43 (2024).
- Antobreh, A. A., Faleide, J. I., Tsikalas, F. & Planke, S. Rift-shear architecture and tectonic development of the Ghana margin deduced from multichannel seismic reflection and potential field data. *Mar. Petrol. Geol.* **26**, 345–368 (2009).
- Meghraoui, M. ICGP-601 Working Group The seismotectonic map of Africa. *Episodes* **39**, 9–18 (2016).
- Irinym, S. A., Lombardi, D. & Ahmad, S. M. Seismic hazard assessment for Guinea, west Africa. *Sci. Rep.* **12**, 2566 (2022).
- Hijma, M. P. et al. A protocol for a geological sea-level database. *Handbook of sea-level research*, pp. 536–553 (2015).
- Engelhart, S. E. & Horton, B. P. Holocene sea level database for the Atlantic coast of the United States. *Quat. Sci. Rev.* **54**, 12–25 (2012).
- García-Artola, A. et al. Holocene sea-level database from the Atlantic coast of Europe. *Quat. Sci. Rev.* **196**, 177–192 (2018).
- Vacchi, M. et al. Postglacial relative sea-level histories along the eastern Canadian coastline. *Quat. Sci. Rev.* **201**, 124–146 (2018).
- Cahill, N., Kemp, A. C., Horton, B. P. & Parnell, A. C. A Bayesian hierarchical model for reconstructing relative sea level: from raw data to rates of change. *Clim* **12**, 525–542 (2016).
- Peltier, W. R., Argus, D. F. & Drummond, R. Space geodesy constrains ice age terminal deglaciation: The global ICE-6G_C (VM5a) model. *J. Geophys. Res.: Solid Earth* **120**, 450–487 (2015).
- Lambeck, K., Rouby, H., Purcell, A., Sun, Y. & Sambridge, M. Sea level and global ice volumes from the Last Glacial Maximum to the Holocene. *Proc. Nat. Acad. Sci.* **111**, 15296–15303 (2014).
- Lambeck, K., Purcell, A. & Zhao, S. The North American Late Wisconsin ice sheet and mantle viscosity from glacial rebound analyses. *Quat. Sci. Rev.* **158**, 172–210 (2017).
- Clark, P. U. et al. The last glacial maximum. *Science* **325**, 710–714 (2009).
- Harrison, S., Smith, D. E. & Glasser, N. F. Late Quaternary meltwater pulses and sea level change. *J. Quat. Sci.* **34**, 1–15 (2009).
- Hanebuth, T. J., Stattegger, K. & Bojanowski, A. Termination of the Last Glacial Maximum sea-level lowstand: The Sunda-Shelf data revisited. *Glob. Plan. Ch.* **66**, 76–84 (2009).

29. Blanchon, P., Medina-Valmaseda, A. & Hibbert, F. D. Revised post-glacial sea-level rise and meltwater pulses from Barbados. *Open Quat* **7**, 1–12 (2021).
30. Barber, D. C. et al. Forcing of the cold event of 8,200 years ago by catastrophic drainage of Laurentide lakes. *Nature* **400**, 344–348 (1999).
31. Li, Y. X., Törnqvist, T. E., Nevitt, J. M. & Kohl, B. Synchronizing a sea-level jump, final Lake Agassiz drainage, and abrupt cooling 8200 years ago. *Earth Plan. Sci. Lett.* **315**, 41–50 (2012).
32. Rush, G. et al. The magnitude and source of meltwater forcing of the 8.2 ka climate event constrained by relative sea-level data from eastern Scotland. *Quat. Sci. Adv.* **12**, 100119 (2023).
33. Törnqvist, T. E. & Hijma, M. P. Links between early Holocene ice-sheet decay, sea-level rise and abrupt climate change. *Nat. Geosci.* **5**, 601–606 (2012).
34. Hijma, M. P. & Cohen, K. M. Holocene sea-level database for the Rhine-Meuse Delta, The Netherlands: implications for the pre-8.2 ka sea-level jump. *Quat. Sci. Rev.* **214**, 68–86 (2019).
35. Smith, D. E., Harrison, S. & Jordan, J. T. Sea level rise and submarine mass failures on open continental margins. *Quat. Sci. Rev.* **82**, 93–103 (2013).
36. Cronin, M. et al. Rapid sea level rise and ice sheet response to 8,200-year climate event. *Geoph. Res. Lett.* **34**, L20603 (2007).
37. Törnqvist, T. E., Bick, S. J., González, J. L., van der Borg, K., & de Jong, A. F. Tracking the sea-level signature of the 8.2 ka cooling event: New constraints from the Mississippi Delta. *Geoph. Res. Lett.* **31**, L23309 (2004).
38. Li, T. et al. Glacial isostatic adjustment modelling of the mid-Holocene sea-level highstand of Singapore and Southeast Asia. *Quat. Sci. Rev.* **319**, 108332 (2023).
39. Li, T. et al. Influence of 3D earth structure on glacial isostatic adjustment in the Russian Arctic. *J. Geophys. Res.: Solid Earth* **127**, e2021JB023631 (2022).
40. Parang, S. et al. Constraining models of glacial isostatic adjustment in eastern North America. *Quat. Sci. Rev.* **334**, 108708 (2024).
41. Li, T., Wu, P., Steffen, H. & Wang, H. In search of laterally heterogeneous viscosity models of glacial isostatic adjustment with the ICE-6G_C global ice history model. *Geophys. J. Int.* **214**, 1191–1205 (2018).
42. Déprez, A., Doubre, C., Masson, F. & Ulrich, P. Seismic and aseismic deformation along the East African Rift System from a reanalysis of the GPS velocity field of Africa. *Geoph. J. Int.* **193**, 1353–1369 (2013).
43. Carlson, A. E., & Clark, P. U. Ice sheet sources of sea level rise and freshwater discharge during the last deglaciation. *Rev. Geophys.*, **50** (2012).
44. Jones, R. S. et al. Stability of the Antarctic Ice Sheet during the pre-industrial Holocene. *Nat. Rev. Earth Env.* **3**, 500–515 (2022).
45. Bradley, S. L., Hindmarsh, R. C., Whitehouse, P. L., Bentley, M. J. & King, M. A. Low post-glacial rebound rates in the Weddell Sea due to Late Holocene ice-sheet readvance. *Earth Plan. Sci. Lett.* **413**, 79–89 (2015).
46. Stokes, C. R. et al. Response of the East Antarctic Ice Sheet to past and future climate change. *Nature* **608**, 275–286 (2022).
47. Bentley, M. J. et al. Mechanisms of Holocene palaeoenvironmental change in the Antarctic Peninsula region. *Holocene* **19**, 51–69 (2009).
48. Anderson, J. B. et al. Ross Sea paleo-ice sheet drainage and deglacial history during and since the LGM. *Quat. Sci. Rev.* **100**, 31–54 (2014).
49. Frieler, K. et al. Consistent evidence of increasing Antarctic accumulation with warming. *Nat. Clim. Ch.* **5**, 348–352 (2015).
50. Caron, L., Métivier, L., Greff-Lefftz, M., Fleitout, L. & Rouby, H. Inverting Glacial Isostatic Adjustment signal using Bayesian framework and two linearly relaxing rheologies. *Geophys. J. Int.* **209**, 1126–1147 (2017).
51. Whitehouse, P. L., Bentley, M. J. & Le Brocq, A. M. A deglacial model for Antarctica: geological constraints and glaciological modelling as a basis for a new model of Antarctic glacial isostatic adjustment. *Quat. Sci. Rev.* **32**, 1–24 (2012).
52. Shennan, I., Long, A. J., & Horton, B. P., Handbook of Sea-level Research. John Wiley Sons. 581 pp (2015).
53. Drechsel, J., Khan, N. S. & Rovere, A. PALEO-SEAL: A tool for the visualization and sharing of Holocene sea-level data. *Quat. Sci. Rev.* **259**, 106884 (2021).
54. Faure, H., Fontes, J. C., Hébrard, L., Monteillet, J. & Pirazzoli, P. A. Geoidal change and shore-level tilt along Holocene estuaries: Senegal River area, West Africa. *Science* **210**, 421–423 (1980).
55. Ausseil-Badie, J. et al. Holocene deltaic sequence in the Saloum Estuary, Senegal. *Quat. Res.* **36**, 178–194 (1991).
56. Lezine, A. M., Turon, J. L. & Buchet, G. Pollen analyses off Senegal: evolution of the coastal palaeoenvironment during the last deglaciation. *J. Quat. Sci.* **10**, 95–105 (1995).
57. Barusseau, J. P. et al. Coastal evolution in Senegal and Mauritania at 103, 102 and 101-year scales: natural and human records. *Quat. Int.* **29**, 61–73 (1995).
58. Martin, L. & Tastet, J. P. Le quaternaire du littoral et du plateau continental de côte d’ivoire rôle des mouvements tectoniques et eustatiques. *Bull. ASEQUA* **33–34**, 17–32 (1972).
59. Giresse, P. & Ngueutchoua, G. Variations des lignes de rivage du plateau continental du Cameroun a la fin du Pleistocene (40 ka a 10 ka BP); chronologie et environnements sédimentaires. *Bull. Soc. Géol. Fr.* **169**, 315–325 (1998).
60. Giresse, P., Malounguila-N’Ganga, D. & Barusseau, J. P. Submarine evidence of the successive shorefaces of the Holocene transgression off southern Gabon and Congo. *J. Coast. Res.* **1**, 61–71 (1986).
61. Delibrias, G., Ortlieb, L. & Petit-Maire, N. New ¹⁴C data for the Atlantic Sahara (Holocene): tentative interpretations. *J. Hum. Evol.* **5**, 535–546 (1976).
62. Giresse, P., Kouyoumontzakis, G. & Delibrias, G. La transgression finiholocene en Angola, aspects chronologique, eustatique, paleoclimatique et epirogenique. *CR Acad. Sci.* **283**, 1157–1160 (1976).
63. Lefèvre, D. & Raynal, J. P. Les formations quaternaires de Casablanca et la chronostratigraphie du Quaternaire marin du Maroc revisitées. *Quaternaire* **13**, 9–21 (2002).
64. Anthony, E. J. & Blivi, A. B. Morphosedimentary evolution of a delta-sourced, drift-aligned sand barrier-lagoon complex, western Bight of Benin. *Mar. Geol.* **158**, 161–176 (1999).
65. Laborel, J. & Delibrias, G. Niveaux marins récents à Vermetidae du littoral ouest-africain. Description, datation et comparaison avec les niveaux homologues des côtes du Brésil. *Bull. ASEQUA* **47**, 97–110 (1976).
66. Talbot, M. R. Holocene changes in tropical wind intensity and rainfall: evidence from southeast Ghana. *Quat. Res.* **16**, 201–220 (1981).
67. Paradis, G. Interprétation paléocéologique et paléogéographique des Taphocénoses de l’Holocène récent du Sud-Bénin, à partir de la répartition actuelle des mollusques littoraux et lagunaires d’Afrique occidentale. *Géobios* **11**, 867–891 (1978).
68. Diara, M. & Barusseau, J. P. Late Holocene evolution of the Salum-Gambia double delta (Senegal). *Geo Eco Marina* **12**, 17–28 (2006).
69. McMaster, R. L., Lachance, T. P. & Ashraf, A. Continental shelf geomorphic features off portuguese guinea, guinea, and sierra leone (west africa). *Mar. Geol.* **9**, 203–213 (1970).
70. Martin, L. & Delibrias, G. Schéma des variations du niveau de la mer en Côte d’Ivoire depuis 25 000 ans. *CR Acad. Sci. serie D* **274**, 2848–2851 (1972).
71. Malounguila-Nganga, D., Giresse, P., Boussafir, M. & Miyouna, T. Late Holocene swampy forest of Loango Bay (Congo). Sedimentary environments and organic matter deposition. *J. Afr. Earth Sci.* **134**, 419–434 (2017).

72. Lézine, A. M. & Chateaufneuf, J. J. Peat in the “Niayes” of Senegal: depositional environment and Holocene evolution. *J. Afr. Earth Sci.* **12**, 171–179 (1991).
73. Peyrot, B. Nouvelles donnees sur la prehistoire du littoral au Gabon. *Les Cahiers D'outre-mer* **38**, 88–93 (1985).
74. Barusseau, J. P., Vernet, R., Saliège, J. F., & Descamps, C. Late Holocene sedimentary forcing and human settlements in the Jerf el Oustani-Ras el Sass region (Banc d'Arguin, Mauritania). *Géomorphologie* **13**, <https://doi.org/10.4000/geomorphologie.634> (2007).
75. Certain, R. et al. New evidence of relative sea-level stability during the post-6000 Holocene on the Banc d'Arguin (Mauritania). *Mar. Geol.* **395**, 331–345 (2018).
76. Cooper, J. A. G., Green, A. N. & Compton, J. S. Sea-level change in southern Africa since the Last Glacial Maximum. *Quat. Sci. Rev.* **201**, 303–318 (2018).
77. Pomel, R. S. Processus épeirogéniques et eustatiques en Basse Côte-d'Ivoire depuis 5000 ans BP (étude radiométrique). *Bull. Ass. Géog. Fr.* **54**, 51–58 (1977).
78. Vacchi, M. et al. Multiproxy assessment of Holocene relative sea-level changes in the western Mediterranean: Sea-level variability and improvements in the definition of the isostatic signal. *Earth-Sci. Rev.* **155**, 172–197 (2016).
79. Reimer, P. J. et al. The IntCal20 Northern Hemisphere radiocarbon age calibration curve (0–55 cal kBP). *Radiocarbon* **62**, 725–757 (2020).
80. Hogg, A. et al. SHCal20 Southern Hemisphere calibration, 0–55,000 years cal BP. *Radiocarbon* **62**, 759–778 (2020).
81. Heaton, T. J. et al. Marine20—the marine radiocarbon age calibration curve (0–55,000 cal BP). *Radiocarbon* **62**, 779–820 (2020).
82. Törnqvist, T. E., Rosenheim, B. E., Hu, P., & Fernandez, A. B. Radiocarbon dating and calibration. *Handbook of Sea-Level Research*, 349–360 (2015).
83. Dey, D. K., Ghosh, S. K. and Mallick, B. K., Generalized Linear Models: A Bayesian Perspective. *Biostatistics* 5. Dekker, New York (2000).
84. Farrell, W. E. & Clark, J. A. On postglacial sea level. *Geophys. J. Int.* **46**, 647–667 (1976).
85. Spada, G. & Melini, D. SELEN 4 (SELEN version 4.0): a Fortran program for solving the gravitationally and topographically self-consistent sea-level equation in glacial isostatic adjustment modeling. *Geosci. Mod. Dev.* **12**, 5055–5075 (2019).
86. Spada, G. & Stocchi, P. SELEN: A Fortran 90 program for solving the “sea-level equation”. *Comp. Geosci.* **33**, 538–562 (2007).
87. Mitrovica, J. X. & Milne, G. A. Glaciation-induced perturbations in the Earth's rotation: A new appraisal. *J. Geoph. Res.: Solid Earth* **103**, 985–1005 (1998).
88. Peltier, W. R. Global glacial isostasy and the surface of the ice-age Earth: the ICE-5G (VM2) model and GRACE. *Annu. Rev. Earth Planet. Sci.* **32**, 11–149 (2004).
89. Roy, K. & Peltier, W. R. Space-geodetic and water level gauge constraints on continental uplift and tilting over North America: regional convergence of the ICE-6G_C (VM5a/VM6) models. *Geophys. J. Int.* **210**, 1115–1142 (2017).
90. Amante, C., & Eakins, B. ETOPO1 Arc-Minute Global Relief Model: Procedures, Data Source and Analysis. NOAA Technical Memorandum NESDIS NGDC-2; National Geophysical Data Center: Boulder, CO, USA; pp. 1–19. (2009).
91. Fretwell, P. et al. Bedmap2: improved ice bed, surface and thickness datasets for Antarctica. *Cryosphere* **7**, 375–393 (2013).
92. Bard, E. et al. Deglacial sea-level record from Tahiti corals and the timing of global meltwater discharge. *Nature* **382**, 241–244 (1996).

Acknowledgements

This work contributes to the bilateral agreement CNR Italy-CNRST Morocco entitled “Quantitative reconstruction of Late Quaternary paleo-shoreline and paleo- environment along the Atlantic coast of Morocco”. B.P.H., T.A.S. and T.L. are supported by the Ministry of Education, Singapore, under its AcRF Tier 3 Award MOE2019-T3-1-004 and Tier 2 Award MOE-T2EP50120-0007. GS is supported by a DIFA RFO grant. This work is Earth Observatory of Singapore contribution number 613. Authors acknowledge PALSEA, a working group of the International Union for Quaternary Sciences (INQUA) and Past Global Changes (PAGES).

Author contributions

M.V., T.A.S. and B.P.H. designed the whole study and wrote the first draft of the manuscript. G.S., D.M. and T.L. led the GIA modelling and analyses. M.V. and E.J.A. compiled the RSL database along the Atlantic coast Africa. M.V. and N.C. performed the statistical analysis. M.V., T.A.S. and B.P.H. provided feedback on the data analyses and interpretation of results. M.V., T.A.S., E.J.A., G.S., D.M., T.L., N.C. and B.P.H. contributed to the improvement of the text.

Competing interests

The authors declare no competing interests.

Additional information

Supplementary information The online version contains supplementary material available at <https://doi.org/10.1038/s41467-025-56721-0>.

Correspondence and requests for materials should be addressed to Matteo Vacchi.

Peer review information *Nature Communications* thanks Fiona Hibbert and the other, anonymous, reviewer(s) for their contribution to the peer review of this work. A peer review file is available.

Reprints and permissions information is available at <http://www.nature.com/reprints>

Publisher's note Springer Nature remains neutral with regard to jurisdictional claims in published maps and institutional affiliations.

Open Access This article is licensed under a Creative Commons Attribution-NonCommercial-NoDerivatives 4.0 International License, which permits any non-commercial use, sharing, distribution and reproduction in any medium or format, as long as you give appropriate credit to the original author(s) and the source, provide a link to the Creative Commons licence, and indicate if you modified the licensed material. You do not have permission under this licence to share adapted material derived from this article or parts of it. The images or other third party material in this article are included in the article's Creative Commons licence, unless indicated otherwise in a credit line to the material. If material is not included in the article's Creative Commons licence and your intended use is not permitted by statutory regulation or exceeds the permitted use, you will need to obtain permission directly from the copyright holder. To view a copy of this licence, visit <http://creativecommons.org/licenses/by-nc-nd/4.0/>.

© The Author(s) 2025